Sub- and near-barrier reactions for $^{12}C+^{108,110}Pd$ and $^{7}Li+^{113,115}In$

O. A. Capurro, D. E. DiGregorio, S. Gil, D. Abriola, M. di Tada, J. O. Fernández Niello, A. O. Macchiavelli,* G. V. Martí, A. J. Pacheco, J. E. Testoni, D. Tomasi, and I. Urteaga

Laboratorio TANDAR, Departamento de Física, Comisión Nacional de Energía Atómica, Av. del Libertador 8250, 1429 Buenos Aires, Argentina

(Received 7 September 1995)

Evaporation-residue and transfer reaction cross sections have been measured for $^{12}C+^{108,110}Pd$ and $^{7}Li+^{113,115}In$. The residual nuclei were detected and identified by off-line observation of the γ rays emitted in their radioactive decays. The $3n$ evaporation channel is the dominant decay mode following the fusion of $^{12}C+^{110}Pd$ and $^{7}Li+^{115}In$ at sub- and near-barrier energies, and $^{12}C+^{108}Pd$ and $^{7}Li+^{113}In$ at bombarding energies just above the Coulomb barrier. The experimental evaporation-residue excitation functions are compared with calculations obtained using simplified coupled-channel and statistical models. In these calculations it is not necessary to include transfer channels to explain the data in the case of $^{12}C+^{110}Pd$ and $^{12}C+^{108}Pd$ but they must be taken into account for $^{7}Li+^{115}In$ and $^{7}Li+^{113}In$.

PACS number(s): 25.70.Hi, 24.10.Eq, 25.70.Gh, 25.70.Jj

I. INTRODUCTION

In recent years, there has been considerable interest in the study of heavy-ion reactions at sub-barrier energies because of the significant enhancement of fusion cross sections over the expectations from one-dimensional barrier penetration models. This enhancement has been ascribed to the coupling of the relative-motion coordinate in the entrance channel to other degrees of freedom (static deformation, vibration, and transfer). The inclusion of coupling produces energy-shifted barriers that result in an increase of the barrier penetration probabilities. All these and other considerations have been extensively discussed in a recent review article [1].

In the present work, we report experimental data on cross sections for the production of evaporation residues and for transfer reactions in four systems: $^{12}C+^{110}Pd$, $^{12}C+^{108}Pd$, $^{7}Li+^{115}In$, and $^{7}Li+^{113}In$. The $3n$ evaporation channel is the most important decay mode of the compound nucleus in all the systems. The experimental evaporation-residue excitation functions are compared with the predictions of a schematic coupled-channel calculation combined with a statistical model. The effect of the coupling to the vibrational degrees of freedom of these target nuclei is small due to the relatively small Coulomb barriers of the systems [2]. Therefore, one would expect that the effect of the coupling to the transfer channels on the fusion cross sections can be easily isolated. This assumption was tested in this paper.

The evaporation-residue and transfer reaction cross sections were determined through off-line observation of delayed γ-ray emission. This experimental technique has been applied in the study of fusion and transfer reactions in several systems (Refs. [3–7]). In Sec. II the experimental procedure is described. The analysis and interpretation of the experimental results for each system are given in Sec. III. Finally, Sec. IV summarizes the conclusions.

II. THE EXPERIMENTAL METHOD

The experiments were carried out at the 20-UD tandem accelerator of the TANDAR Laboratory in Buenos Aires. Beams of ^{12}C with laboratory energies from 36.5 to 54 MeV were used to bombard thin targets of enriched metallic palladium (200 $\mu g/cm^2$ thick, 96.98% ^{110}Pd and 2.35% ^{108}Pd). These targets were prepared by dilution of enriched metallic palladium in nitric acid and deposited on carbon foils 40 $\mu g/cm^2$ thick. The evaporation and transfer residues were collected by aluminum foils with thicknesses of 650-950 $\mu g/cm^2$. Targets of natural indium (200 $\mu g/cm^2$, 95.7% ^{115}In and 4.3% ^{113}In) were bombarded with ^{7}Li ions with laboratory energies ranging from 20.4 to 37.1 MeV. These targets were made by vacuum evaporation onto 900-$\mu g/cm^2$-thick aluminum films. This backing also acts as a catcher foil. To verify that none of the evaporation and transfer residues were lost, a second catcher foil was added behind the first one at the highest bombarding energy in all systems.

During the bombardments, two silicon surface-barrier detectors were used to monitor the elastic scattering. For the $^{7}Li+^{113,115}In$ systems, both detectors were placed at $\pm 30°$ relative to the beam direction. Since at this angle the cross section for elastic scattering follows the Rutherford formula, and the solid angles of the monitor detectors were known, it was possible to obtain an absolute measurement of the cross sections independent of the target thickness and of the integrated beam current. For the systems $^{12}C+^{108,110}Pd$, in order to avoid possible overlap between the elastic peaks coming from the target and from the catcher, one detector was placed at 30° and the other at 90° where only the peak corresponding to the palladium is present. Short irradiations without the catcher foils allow the determination of the ratio between the elastic scattering cross sections at 90° and the pure Rutherford cross sections at 30°. These ratios permit one to monitor the beam intensity through the counting rate corresponding to backward elastic scattering, given by the 90° detector when target and catcher foils are placed at the appropriate angles relative to the beam direction. The beam intensity

*Permanent address: Lawrence Berkeley Laboratory, Berkeley, California 94720.

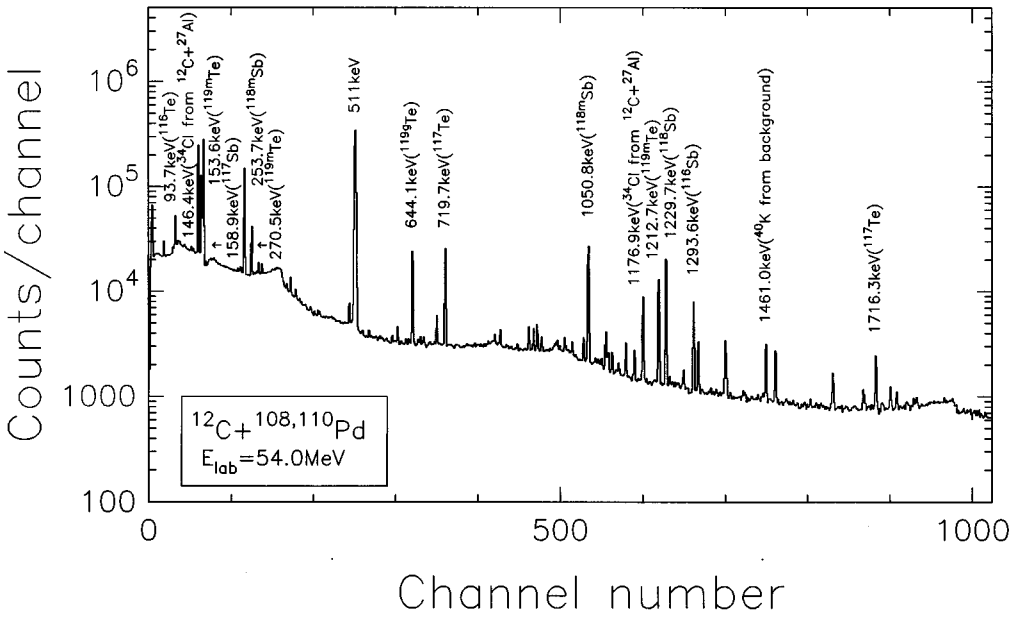

FIG. 1. Off-line energy spectrum obtained with an intrinsic Ge detector for $^{12}C+^{108,110}Pd$ at the highest laboratory bombarding energy (54.0 MeV) showing the delayed γ rays emitted from the radioactive residues.

during the bombardments was recorded by multiscaling in one-minute intervals the integrated current in a Faraday cup.

Following irradiations of about 2–10 h at intensities of $\sim$100 nA (electric), the catcher foils were removed from the scattering chamber and placed in front of a high-purity intrinsic germanium detector. The γ rays resulting from the activated foils were counted off line and the corresponding energy spectra were accumulated and recorded automatically at various time intervals during several hours. Figures 1 and 2 show two typical spectra associated with the decay of the different radioactive residues obtained for $^{12}C+^{108,110}Pd$ at E_{lab} = 54.0 MeV and for $^{7}Li+^{113,115}In$ at E_{lab} = 37.1 MeV, respectively. A large number of γ rays can be observed in the spectra, which covered the photon-energy range from 70 to 2000 keV. γ rays are labeled with the decay energy (in keV) and the parent nucleus or the reaction channel. The HPGe detector achieved an energy resolution of 2.0 keV [full width at half maximum (FWHM)] at 1332.5 keV. The absolute photopeak efficiency of the detector, which was obtained using a set of calibrated sources, was determined with an accuracy of $\pm$4% in the energy range from 200 to 2000 keV while it was estimated to be $\sim$15% for energies below 200 keV.

Given the known half-lives and absolute γ-ray intensities taken from Ref. [8], it was possible to obtain the production rates of the parent nuclei and, hence, the cross sections. The production rates were determined from the peak areas of the γ rays, taking into account the detector efficiency and by extrapolating the decay curves at the end of the bombardment. An absolute measurement of the evaporation-residue

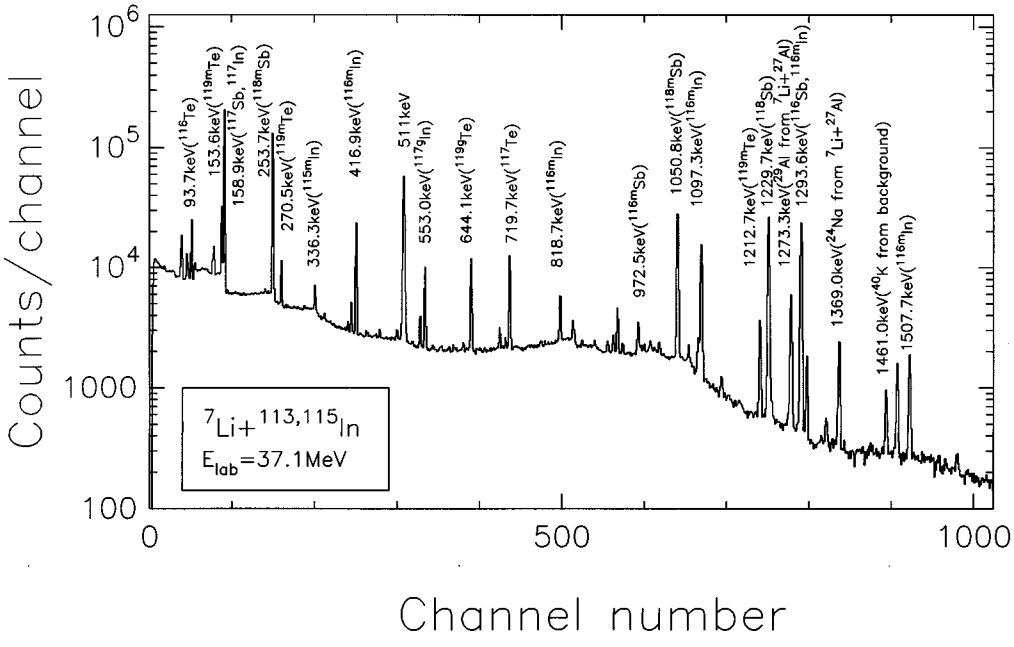

FIG. 2. Off-line energy spectrum obtained with an intrinsic Ge detector for $^{7}Li+^{113,115}In$ at the highest laboratory bombarding energy (37.1 MeV) showing the delayed γ rays emitted from the radioactive residues.

TABLE I. Experimental fusion-evaporation cross sections for $^{12}C+^{110}Pd$.

$E_{c.m.}$ (MeV)	^{119}Te σ_{3n} (mb)	^{118m}Sb $\sigma_{p3n(m.s.)}$ (mb)[a]
48.7	156.1 ± 1.2	12.81 ± 0.06
46.0	190.6 ± 1.0	5.38 ± 0.03
43.3	235.9 ± 1.5	1.64 ± 0.05
41.5	203.6 ± 0.9	0.52 ± 0.03
39.7	145.9 ± 1.4	0.12 ± 0.03
37.9	101.4 ± 1.5	
37.0	56.32 ± 0.59	
36.1	36.65 ± 0.81	
35.2	11.92 ± 0.21	
34.7	6.85 ± 0.11	
34.3	3.26 ± 0.12	
33.8	1.87 ± 0.08	
33.4	0.81 ± 0.07	

[a]These cross sections correspond to the formation of the metastable state (m.s.).

and transfer reaction cross sections was obtained by normalizing to Rutherford scattering. The measured evaporation-residue cross sections are listed in Tables I to III, and V. Table IV includes the experimental transfer and inelastic scattering cross sections for $^{7}Li+^{115}In$. The center-of-mass bombarding energies given in these tables correspond to the energy at the center of the target. The uncertanties in the tables include statistical errors.

There are several sources of error that contribute to the uncertainty in the cross sections. Systematic errors arise from both the absolute Rutherford normalization ($< 6\%$) and the detector efficiency (quoted above). Uncertainties in the absolute intensity of the γ transitions of the radioactive isotopes ($< 1\%$) are partly random and partly systematic in nature. Purely statistical errors come from the determination of the peak areas ($< 5\%$). The addition in quadrature of random and partially random errors yields an overall uncertainty of about 5.1% in the cross sections. The uncertainty in the beam energy was determined to an accuracy of 1%.

TABLE II. Experimental fusion-evaporation cross sections for $^{12}C+^{108}Pd$.

$E_{c.m.}$ (MeV)	^{117}Te σ_{3n} (mb)	^{117}Sb σ_{p2n} (mb)	^{116}Te σ_{4n} (mb)	^{116m}Sb $\sigma_{p3n(m.s.)}$ (mb)[a]
48.6	368.3 ± 4.7	148.8 ± 4.0	104.2 ± 2.5	17.5 ± 3.5
45.9	316.3 ± 2.5	123.2 ± 2.1	38.7 ± 1.4	7.7 ± 2.2
43.2	312.5 ± 3.9	75.7 ± 3.5	16.1 ± 2.4	
41.4	221.4 ± 2.8	73.1 ± 2.3	9.1 ± 1.2	
39.6	137.5 ± 3.1	38.2 ± 2.7		
37.8	88.9 ± 4.1	17.6 ± 3.4		
36.9	30.9 ± 2.8			
36.0	21.6 ± 2.3	7.5 ± 1.9		
35.1	11.5 ± 2.5			
34.7	0.16 ± 0.04			

[a]These cross sections correspond to the formation of the metastable state (m.s.).

TABLE III. Experimental fusion-evaporation cross sections for $^{7}Li+^{115}In$.

$E_{c.m.}$ (MeV)	^{119}Te σ_{3n} (mb)	^{118m}Sb σ_a (mb)+ σ_b (mb)[a]
35.0	220.2 ± 5.7	80.01 ± 0.25
32.3	311.2 ± 6.3	47.56 ± 0.23
29.6	462.2 ± 6.0	34.43 ± 0.20
27.8	528.2 ± 9.5	29.92 ± 0.26
26.0	524.9 ± 5.9	21.85 ± 0.16
24.2	442.3 ± 5.8	15.3 ± 1.2
22.4	295.9 ± 4.4	9.20 ± 0.12
21.5	232.8 ± 3.6	6.85 ± 0.12
20.6	155.9 ± 3.4	4.26 ± 0.09
20.1	112.4 ± 2.9	2.97 ± 0.09
19.7	72.1 ± 2.9	2.16 ± 0.10
19.2	56.1 ± 1.9	1.40 ± 0.06

[a]These cross sections correspond to the formation of the metastable state, σ_a for the $p3n$ fusion-evaporation reaction, and σ_b for the $2pn$ stripping transfer reaction.

III. RESULTS AND DISCUSSION

To illustrate the radioactive isotopes studied in this work, Fig. 3 displays the region of interest in the chart of nuclides. All observed radioactive evaporation and transfer residues produced in the $^{12}C+^{108,110}Pd$ and $^{7}Li+^{113,115}In$ systems are underlined in this figure.

The experimental excitation functions are shown in Figs. 4–8. The $3n$ evaporation channel is the strongest decay mode in all the systems. The error bars in the figures only include statistical errors.

The fusion-evaporation experimental results were compared with model calculations. For this purpose it was necessary to relate a fusion cross section and a spin distribution for the compound nucleus to the evaporation channel cross sections. This was done by combining a schematic coupled-

TABLE IV. Experimental transfer and inelastic scattering cross sections for $^{7}Li+^{115}In$.

$E_{c.m.}$ (MeV)	^{115m}In $\sigma_{inel(1/2^-)}$ (mb)	$^{116m1}In$ $\sigma_{1n\ stripping}$ (mb)[a]	^{117g}In $\sigma_{2n\ stripping}$ (mb)[b]
35.0	4.32 ± 0.34	54.37 ± 0.64	9.30 ± 0.20
32.3	3.15 ± 0.29	43.40 ± 0.57	9.22 ± 0.20
29.6	3.06 ± 0.37	42.41 ± 0.52	10.66 ± 0.18
27.8	3.66 ± 0.44	42.76 ± 0.85	12.38 ± 0.32
26.0	3.55 ± 0.31	43.52 ± 0.52	12.21 ± 0.18
22.4	2.07 ± 0.21	31.63 ± 0.39	8.49 ± 0.14
21.5	1.69 ± 0.19	28.58 ± 0.40	7.31 ± 0.13
20.6	1.53 ± 0.23	21.81 ± 0.29	4.93 ± 0.10
20.1	1.32 ± 0.19	17.91 ± 0.36	3.80 ± 0.11
19.7	1.02 ± 0.20	17.64 ± 0.41	3.61 ± 0.14
19.2	0.76 ± 0.11	12.56 ± 0.25	2.23 ± 0.08

[a]These cross sections correspond to the formation of the two metastable states.

[b]These cross sections correspond to the partial formation of the metastable state and total population of the ground state.

^{116}Te 2.49h	^{117}Te 1.03h	^{118}Te 6.00d	^{119}Te m 4.69d / g 16.1h	^{120}Te stable	^{121}Te m 154d / g 16.8d	^{122}Te stable
^{115}Sb 32.1m	^{116}Sb m 1.01h / g 15.8m	^{117}Sb 2.80h	^{118}Sb m 5.00h / g 3.6m	^{119}Sb 1.59d	^{120}Sb m 5.76d / g 15.9m	^{121}Sb stable
^{114}Sn stable	^{115}Sn stable	^{116}Sn stable	^{117}Sn m 13.6d / g stable	^{118}Sn stable	^{119}Sn m 293d / g stable	^{120}Sn stable
^{113}In m 1.66h / g stable	^{114}In m 49.5d / g 71.9s	^{115}In m 4.49h / g ~stable	^{116}In m2 2.18s / m1 54.2m / g 14s	^{117}In m 1.94h / g 43.8m	^{118}In m2 8.5s / m1 4.45m / g 5.0s	^{119}In m 18.0m / g 2.4m

FIG. 3. Region of the chart of the nuclides relevant to this work. The observed radioactive isotopes are indicated by underlined symbols.

channel model, which gives the fusion cross sections and spin distributions, with a statistical model, which gives the probability of each evaporation channel.

The first step in the calculations was performed using a modified version of the code CCDEF [9]. When this code is used in the no-coupling mode, two out of the three parameters of the nuclear potential (the depth, the diffuseness, and the radius) are considered as free parameters to be obtained from a least-squares fit to the corresponding experimental points at energies above the Coulomb barrier for each system. In this region, the coupling to other degrees of freedom (deformation, vibration, and transfer) has little influence. In our calculations, we have considered couplings to vibrational states of the target nuclei. The corresponding deformation parameters were obtained from Ref. [10]. The coupling to inelastic excitations of the projectile nuclei has been neglected because of the high quadrupole transition energies. Coupling to transfer channels was included when it was suitable. The statistical decay of the compound nucleus was calculated using the computer code PACE with default input parameters [11]. The most relevant parameters are the level density parameter (a_n = A/7.5 [MeV^{-1}]) and the reduced γ transition strengths. We have used 0.000 01, 0.01, 5.9, and 0.000 88 Weisskopf units (W.u.) for the E1, M1, E2, and M2 transitions, respectively.

TABLE V. Experimental fusion-evaporation cross sections for ^{7}Li+^{113}In.

	^{117}Te	^{116}Te	^{116m}Sb
$E_{\text{c.m.}}$ (MeV)	σ_{3n} (mb)	σ_{4n} (mb)	$\sigma_{p3n(\text{m.s.})}$ (mb)[a]
34.9	461.3 ± 7.6	351.2 ± 6.9	87.8 ± 9.7
32.2	436.9 ± 7.1	159.2 ± 6.1	40.3 ± 7.0
29.5	551.0 ± 6.9	52.6 ± 4.3	28.8 ± 4.1
27.7	601. ± 11.	1.25 ± 0.32	0.35 ± 0.18
25.9	514.4 ± 6.5		
22.3	239.5 ± 4.4		
21.4	179.2 ± 4.3		
20.5	97.8 ± 3.0		
20.1	56.5 ± 3.0		
19.6	45.5 ± 3.4		
19.2	24.2 ± 2.2		

[a]These cross sections correspond to the formation of the metastable state (m.s.).

A. The ^{12}C+^{110}Pd system

The measured cross sections for the production of ^{119}Te and ^{118m}Sb are given in Table I and their excitation functions are shown in Fig. 4. The presence of ^{119}Te was observed through the 1212.7 keV (I_γ = 66.7%) and the 644.07 keV (I_γ = 84.5%) transitions from the ground and metastable

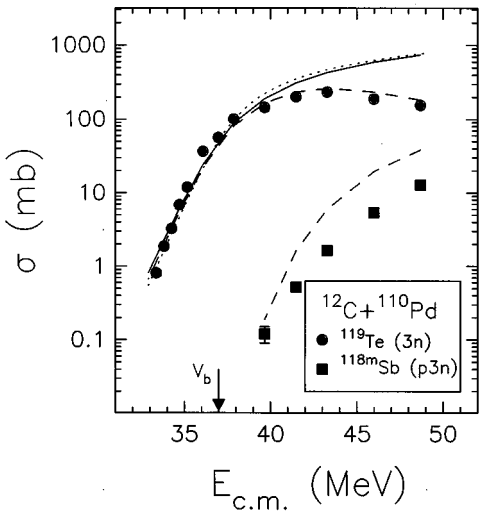

FIG. 4. Experimental excitation functions of the $3n$ and $p3n$ (metastable state) evaporation channels for ^{12}C+^{110}Pd. The solid (dotted) curve is the CCDEF calculation for the fusion cross section with (without) coupling to the inelastic excitation of the target as described in the text. Dashed curves show the fits to the $3n$ and $3pn$ channels obtained by combining the coupled-channel (CCDEF) and the statistical model (PACE) calculations.

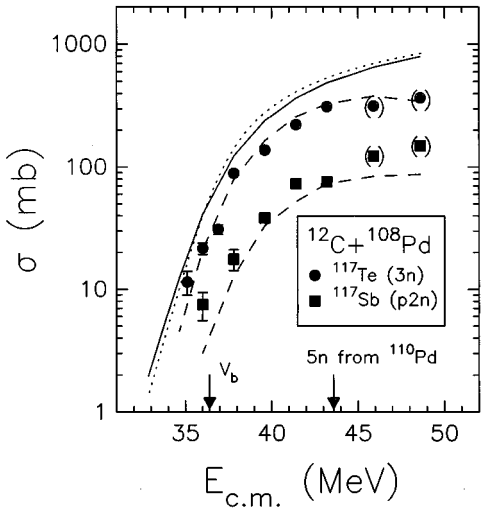

FIG. 5. Experimental excitation functions of the $3n$ and $p2n$ evaporation channels for $^{12}C+^{108}Pd$. Possible spurious contributions are indicated in parentheses (see text). The solid (dotted) curve is the CCDEF calculation for the fusion cross section with (without) coupling to the inelastic excitation of the target as described in the text. Dashed curves correspond to the $3n$ and $p2n$ evaporation channel cross sections calculated using CCDEF and PACE.

states of the nucleus, respectively. Because there is no isomeric transition connecting these states, the cross section of the $3n$ channel was simply calculated by summing the corresponding cross sections obtained from the activities of the mentioned transitions. The decay of ^{118m}Sb was studied through the 253.73 keV (I_γ = 99%) γ transition. The $2n$ channel leads to a stable isotope, ^{120}Te; therefore, it could

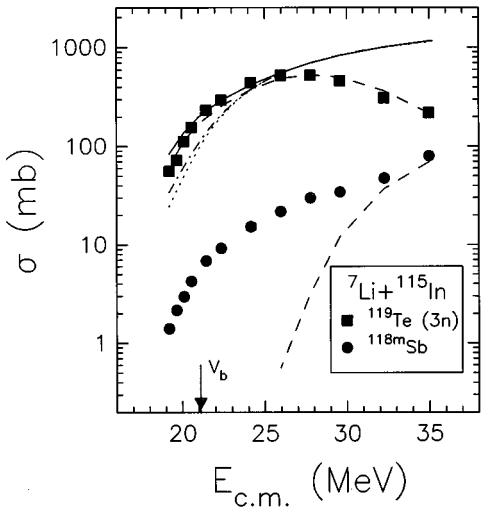

FIG. 6. Experimental excitation functions of the $3n$ evaporation channel and the $p3n$ evaporation channel + $2pn$ transfer channel (both metastable states) for $^{7}Li+^{115}In$. The dot-dashed (dotted) curve represents the CCDEF calculation for the fusion cross section with (without) coupling to the inelastic excitation of the target. The solid line shows the effect of including the coupling to transfer reaction channels. Dashed curves correspond to the $3n$ and $p3n$ evaporation channels cross sections calculated using CCDEF and PACE.

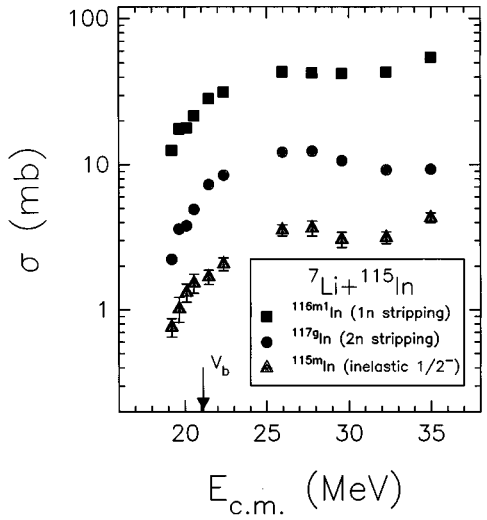

FIG. 7. Experimental $1n$ stripping, $2n$ stripping, and inelastic ($1/2^-$) excitation functions for $^{7}Li+^{115}In$. The $1n$ stripping reaction corresponds to the formation of the two isomeric states ($^{116m1}In$ and $^{116m2}In$). The $2n$ stripping reaction is associated with the total population of the ground state (^{117g}In) and the partial formation of the metastable state (^{117m}In).

not be observed with our technique. Regarding the ^{118}Te nucleus ($4n$ channel), it was not studied because there is no γ emission in its decay path and therefore the activities could not be determined using this method. In principle, one could follow its decay through the daugther nucleus (^{118g}Sb), but the intensities of the emitted γ rays are too small. The decay of ^{119}Sb could not be observed because the energy of the transition involved (23.9 keV) was below our detection threshold.

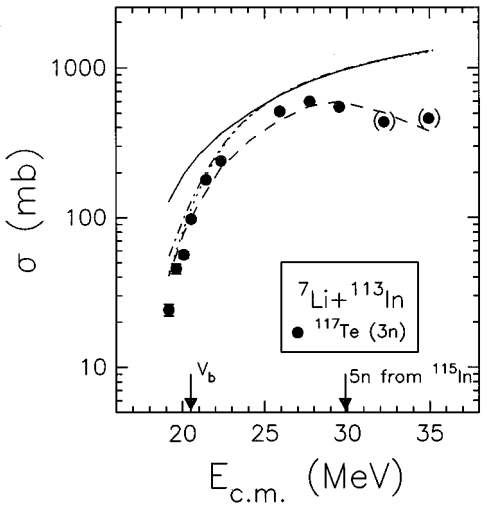

FIG. 8. Experimental $3n$ evaporation channel for $^{7}Li+^{113}In$. Possible spurious contributions are indicated in parentheses (see text). The dot-dashed (dotted) curve represents the CCDEF calculation for the fusion cross section with (without) coupling to the inelastic excitation of the target. The solid line shows the effect of including the coupling to the transfer reaction channels. Dashed curve corresponds to the $3n$ evaporation channel cross section calculated using CCDEF and PACE.

The dotted curve in Fig. 4 represents the CCDEF calculation of the fusion cross section corresponding to the uncoupled case. The values for the height and the position of the barrier are $V_b = 37.0$ MeV and $R_b = 10.22$ fm. The full curve is the prediction of CCDEF when one includes the coupling to the first 2^+ state of ^{110}Pd ($E_{2+} = 0.3738$ MeV, $\beta_2 = 0.257$). The dashed curves correspond to the $3n$ and $p3n$ channels cross sections obtained through the statistical model calculation (PACE) using the spin distribution resulting from CCDEF for the coupling case. The agreement for the $3n$ channel is quite good. As can be seen in Fig. 4, the coupling to the inelastic excitation of the target nucleus is barely appreciable at sub-barrier energies.

B. The ^{12}C+^{108}Pd system

The absolute cross sections for the evaporation residues measured in this system are listed in Table II. The excitation functions corresponding to the ^{117}Te and ^{117}Sb residues are plotted in Fig. 5. The activities for the decay of the ^{117}Te, ^{117}Sb, ^{116}Te, and ^{116m}Sb nuclei were determined by analyzing the 719.7 keV ($I_\gamma = 64.7\%$), 158.56 keV ($I_\gamma = 85.9\%$), 93.74 keV ($I_\gamma = 32.1\%$), and 972.54 keV ($I_\gamma = 72.0\%$) γ transitions, respectively. The experimental cross sections of the $3n$ channel at the two highest energies could have some contribution coming from the $5n$ channel in the ^{12}C+^{110}Pd system, since ^{110}Pd is also present in the target. Since ^{117}Sb is also fed by its parent ^{117}Te, this additional contribution was subtracted. There are three isotopes whose decay paths proceed through the same γ transition (158.56 keV): ^{117m}In, ^{117g}In, and ^{117m}Sn. However, the contribution from ^{117m}Sn with a 13.61 days half-life can be neglected since our measurements lasted less than 4 h. The other two contributions from ^{117m}In and ^{117g}In can be safely ignored since we did not find pure γ transitions of such isotopes in the spectra.

In Fig. 5, the dotted curve corresponds to the CCDEF calculation of the fusion cross section without couplings. The barrier parameters are $V_b = 36.4$ MeV and $R_b = 10.45$ fm. The full curve is the result obtained when adding the coupling to the first excited state of the target nucleus (^{108}Pd, $E_{2+} = 0.4339$ MeV, $\beta_2 = 0.243$). The dashed curves are the predictions for $3n$ and $p2n$ channels using the xn distributions obtained with PACE. This calculation describes reasonably well the experimental $3n$ cross section.

C. The ^{7}Li+^{115}In system

The absolute evaporation-residue and transfer cross sections are reported in Tables III and IV, and are shown as a function of bombarding energy in Figs. 6 and 7, respectively. The ^{7}Li+^{115}In system forms the same compound nucleus as the ^{12}C+^{110}Pd system; therefore the same γ transitions were used to extract the corresponding evaporation-residue cross sections. We have also found in the spectra γ rays belonging to the decay of isotopes produced in transfer reactions and inelastic scattering. Thus we measured the activities for ^{115m}In (inelastic scattering), ^{116m1}In (one-neutron stripping), and ^{117g}In (two-neutron stripping) following the decay of the 336.26 keV ($I_\gamma = 45.8\%$), 416.92 keV ($I_\gamma = 29.2\%$), and 552.97 keV ($I_\gamma = 99.7\%$) transitions, respectively. It is to be noticed that the measured activity of the 416.92 keV transition includes the contributions from ^{116m1}In and ^{116m2}In since the $T_{1/2} = 2.18$ s half-life isomer fully decays into the $T_{1/2} = 54.15$ min half-life isomeric state. Thus the $1n$ stripping cross sections are associated with the formation of the two isomers (^{116m1}In and ^{116m2}In). The production of ^{117m}In was barely observed through the 315.22 keV transition, but since the statistics were very poor we were not able to obtain a reliable cross section for this isotope. Therefore, since this metastable state decays to the ground state with a probability of 47%, the activity of the 552.97 keV transition accounts for the formation of ^{117g}In plus some contribution coming from ^{117m}In. Thus the $2n$ stripping cross sections are associated with the total population of the ground state plus the partial formation of the metastable state. Other transfer channels are energetically favored in this system: $1p$ pickup and $1p$, $1pn$, $1p2n$, $2pn$, and $2p2n$ stripping reactions. However, most of these channels cannot be measured through our experimental method. This is so because these transfer channels correspond to stable isotopes (^{114}Cd, ^{116}Sn, ^{118}Sn), and either they have a long half-life compared to the time scale of our experiment (^{117}Sn), or the energy of the transition involved is below the threshold of our detector (^{119}Sb).

The dotted curve in Fig. 6 represents the result of CCDEF for the uncoupled case. The barrier parameters are $V_b = 21.1$ MeV and $R_b = 9.70$ fm. The coupling to the inelastic excitation of ^{115}In was calculated taking an average value of the deformation parameters of the neighboring even-even nuclei for this target (^{116}Sn and ^{114}Cd), as was done in Ref. [12]. This procedure gave a value of $\langle\beta_2\rangle = 0.152$. However, the excitation energy was taken in a different way. A value of $E^* = 0.941$ MeV was chosen because it corresponds to the quadrupole transition ($9/2^+$ to $5/2^+$) [13]. Although the inclusion of such coupling increases the fusion cross section at the lowest energy, it is insufficient to explain the data, as can be seen from the dot-dashed curve in Fig. 6. Since some transfer channels were observed in our spectra, we were led to include couplings to these channels. In our approach, we included the previously mentioned reactions in a single transfer channel with an effective Q value equal to zero. In this way, the only parameter to be adjusted was an effective coupling strength at the barrier position ($F_{\rm eff}$). Although this approximation is rather crude, it turns out quite useful to get a qualitative idea of the effect on fusion arising from the coupling of transfer channels.

Following this procedure and using the xn distributions obtained with PACE, we found that a reasonable fit for the $3n$ channel excitation function can be achieved with $F_{\rm eff} = 2.9$ MeV, as shown in Fig. 6 (dashed curve). The disagreement between the calculated curve for the $p3n$ evaporation channel and the corresponding experimental points suggests that another reaction contributing to the activities for the ^{118m}Sb may be present. A possible contribution could come from the $2pn$ stripping reaction in the ^{7}Li+^{115}In system. As was just pointed out, this transfer channel is energetically favored. On the other hand, such an extra contribution cannot correspond to the ^{113}In(^{7}Li,pn)^{118m}Sb reaction because the subsequent activities should be very low. This is due to the very low concentration (4.3%) of the ^{113}In isotope in the target. Therefore, one can reasonably assume that the extra formation of

^{118m}Sb may come from the $2pn$ stripping reaction in the ^{7}Li+ ^{115}In system.

D. The ^{7}Li+ ^{113}In system

The excitation function for ^{117}Te is shown in Fig. 8. The absolute cross sections for the production of ^{117}Te, ^{116}Te, and ^{116m}Sb are presented in Table V. The fusion of ^{7}Li+ ^{113}In forms the same compound nucleus as ^{12}C+ ^{108}Pd; therefore, we used the same γ transitions (described in Sec. III B) to obtain the corresponding cross sections. As in the ^{12}C+ ^{108}Pd system, the cross sections for ^{117}Te at the highest energies (the two points shown between parentheses in Fig. 8) can have an additional contribution from the $5n$ channel of the ^{7}Li+ ^{115}In system.

In Fig. 8 the dotted curve shows the CCDEF calculation for the no-coupling case. The adopted parameters for the barrier are $V_b = 20.5$ MeV and $R_b = 10.03$ fm. The coupling to the inelastic excitation of the target nucleus was taken into account. Its deformation parameter was chosen by averaging the respective values of the adjacent even-even nuclei (^{114}Sn and ^{112}Cd): $\langle\beta_2\rangle = 0.153$. The energy of the quadrupole transition ($9/2^{+}$ to $5/2^{+}$) is 1.0242 MeV [13]. The dot-dashed curve in Fig. 8 illustrates the results of this calculation. As one can see, this coupling is not enough to explain the observed enhancement below the Coulomb barrier. Then we included coupling to the transfer processes in our calculations as in the ^{7}Li+ ^{115}In system. An identical procedure was followed, replacing the same transfer channels by a single transfer channel with an effective Q value equal to zero. Taking into account the xn distributions calculated with PACE, the best fit for the $3n$ evaporation excitation function was obtained with $F_{\rm eff} = 2.9$ MeV, as can be seen from the dashed curve in Fig. 8.

The formation of the ^{117}Sb nucleus was analyzed through the 158.56 keV transition that belongs also to other decay paths (see Sec. III B). The additional formation coming from its parent nucleus (^{117}Te) was subtracted. Furthermore, it was necessary to take into account the contributions of ^{117m}In and ^{117g}In to the activities of the 158.56 keV transition because pure γ transitions of these nuclei were observed in the spectra. However, if one assumes that the resulting activities only correspond to the $p2n$ evaporation channel, the cross sections of this channel remained much higher than the predictions of our fusion-evaporation calculations (for example, $\sigma_{\rm meas} \sim 700$ mb versus $\sigma_{\rm calc} \sim 100$ mb at $E_{\rm c.m.} = 32.2$ MeV). The reason for this anomalous enhancement might be the presence of other reaction channels. The $2p$ stripping reaction might also be present in the ^{7}Li+ ^{115}In system although this transfer channel is not amongst the most energetically favored. To verify this assumption, we have determined the activities corresponding to the ^{117}Sb nucleus coming from the $p2n$ evaporation channel in the ^{7}Li+ ^{113}In system. These cross sections were estimated using CCDEF and PACE. Then the calculated activities corresponding to this evaporation channel were subtracted from our total measured activities for ^{117}Sb. Thus their cross sections were calculated on the assumption that the resulting activities correspond exclusively to the $2p$ stripping reaction from the ^{7}Li+ ^{115}In system. The $2p$ stripping reaction cross sections deduced in this way look reasonable when compared with the $2pn$ stripping reaction cross sections. In Fig. 9, we present the calculated $p2n$ evaporation channel excitation function in ^{7}Li+ ^{113}In and the deduced $2p$ stripping reaction cross sections in the ^{7}Li+ ^{115}In system. However, it must be taken into account that the cross sections deduced for this channel just have a conjectural character based on the hypothesis of its presence in the ^{7}Li+ ^{115}In system. On the other hand, the calculations performed to evaluate the $p2n$ evaporation channel cross sections in the ^{7}Li+ ^{113}In system are just an estimate based on the statistical model.

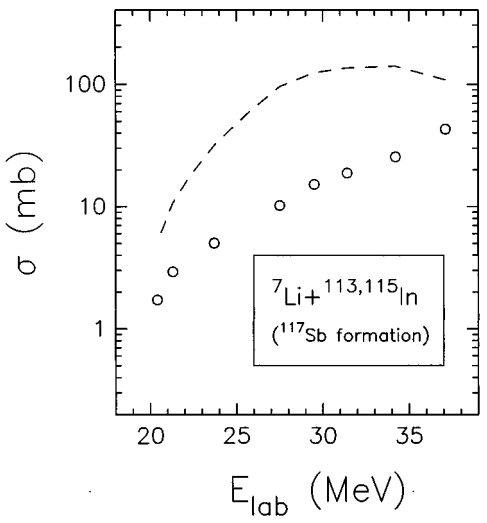

FIG. 9. Dashed curve corresponds to $p2n$ evaporation channel excitation function for ^{7}Li+ ^{113}In obtained by combining coupled-channel (CCDEF) and statistical model (PACE) calculations. The open circles are the deduced $2p$ stripping cross sections for ^{7}Li+ ^{115}In obtained through the calculated cross sections of that reaction and the total measured activity of ^{117}Sb (see text).

IV. SUMMARY

We have measured experimental excitation functions of all observed radioactive isotopes in the following systems: ^{12}C+ ^{110}Pd, ^{12}C+ ^{108}Pd, ^{7}Li+ ^{115}In, and ^{7}Li+ ^{113}In. The $3n$ evaporation channel is the dominant decay mode for the fusion evaporation of ^{12}C+ ^{110}Pd and ^{7}Li+ ^{115}In at sub- and near-barrier energies. The same channel exhausts more than 50% of the total fusion cross section for ^{12}C+ ^{108}Pd and ^{7}Li+ ^{113}In at energies just above the Coulomb barrier. We have compared our experimental results for the $3n$ channel with a simplified coupled-channel (CCDEF) and a statistical model (PACE) calculation. The parameters used in the code PACE were the same for all the systems and were taken from Ref. [11].

The effects of the coupling to the quadrupole oscillations of the participant nuclei are weak due to the small size of the Coulomb barrier [2]. This statement can also be inferred from Ref. [6] where, for a given target, the enhancement of the fusion cross sections decreases as the atomic number of the projectile decreases. Therefore, the study of the present systems provides useful information on the effects of transfer processes on the fusion cross sections. The coupling to the inelastic excitation in ^{12}C+ ^{108,110}Pd has little influence on fusion cross sections at sub-barrier energies. No transfer re-

actions were observed as expected from energetic considerations in these systems. In addition, it was not necessary to include the coupling to transfer channels to explain the data. This has also been observed in the $^{16}O+^{112}Cd$ system [14] where the nuclear structure of the reactants is similar to the $^{12}C+^{108,110}Pd$ systems. The situation is different for the $^{7}Li+^{113,115}In$ system. The fact that coupling to the inelastic excitation was not enough to describe the $3n$ channel experimental cross sections and the presence of transfer channels induced us to couple these processes in the calculations. This produced a reasonable fit to the data. The experimentally observed enhancement of the cross sections over the predictions of one-dimensional barrier penetration at sub-barrier energies is about a factor of 3. Therefore, one could conclude that the enhancement of the fusion cross section due to the coupling to the transfer channels ought to be considered for the $^{7}Li+^{113,115}In$ system, even when small transfer cross sections have been measured in one of them ($^{7}Li+^{115}In$). This is consistent with the observations presented in Ref. [15]. There, small (large) transfer cross sections were correlated with small (large) sub-barrier fusion enhancement.

ACKNOWLEDGMENTS

Some of us (D.E.D.G., M.d.T., J.O.F.N., A.J.P., and J.E.T.) acknowledge the financial support of the Consejo Nacional de Investigaciones Científicas y Técnicas, Argentina.

[1] R. Vandenbosch, Annu. Rev. Nucl. Part. Sci. **42**, 447 (1992).

[2] S. Gil, in *Proceedings of Workshop on Heavy Ion Fusion: Exploring the Variety of Nuclear Properties, Padova, Italy, 1994*, edited by A.M. Stefanini, G. Nebbia, S. Lunardi, G. Montagnoli, and A. Viturri (World Scientific, Singapore, 1994), p. 78.

[3] D.E. DiGregorio, M. di Tada, D. Abriola, M. Elgue, A. Etchegoyen, M.C. Etchegoyen, J.O. Fernández Niello, A. Ferrero, S. Gil, A.O. Macchiavelli, A.J. Pacheco, J.E. Testoni, P.R.S. Gomes, V. Vanin, R. Liguori Neto, E. Crema, and R. G. Stokstad, Phys. Rev. C **39**, 516 (1989).

[4] J.O. Fernández Niello, M. di Tada, A.O. Macchiavelli, A.J. Pacheco, D. Abriola, M. Elgue, A. Etchegoyen, M.C. Etchegoyen, S. Gil, and J.E. Testoni, Phys. Rev. C **43**, 2303 (1991).

[5] D. Tomasi, J.O. Fernández Niello, A.O. Macchiavelli, A.J. Pacheco, J.E. Testoni, D. Abriola, O.A. Capurro, D.E. DiGregorio, M. di Tada, C.P. Massolo, and F. Penayo, Phys. Rev. C **48**, 2840 (1993).

[6] P.R.S. Gomes, I.C. Charret, R. Wanis, G.M. Sigaud, V. Vanin, R. Liguori Neto, D. Abriola, O.A. Capurro, D.E. DiGregorio, M. di Tada, G. Duchene,M. Elgue, A. Etchegoyen, J.O. Fernández Niello, A. Ferrero, S. Gil, A.O. Macchiavelli, A.J. Pacheco, and J.E. Testoni, Phys. Rev. C **49**, 245 (1994).

[7] S. Gil, F. Hasenbalg, J.E. Testoni, D. Abriola, M.C. Berisso, M. di Tada, A. Etchegoyen, J.O. Fernández Niello, A.J. Pacheco, A. Charlop, A.A. Sonzogni, and R. Vandenbosch, Phys. Rev. C **51**, 1336 (1995).

[8] E. Browne and R.B. Firestone, *Table of Radioactive Isotopes* (Wiley-Interscience, New York, 1986).

[9] J.O. Fernández Niello, C.H. Dasso, and S. Landowne, Comput. Phys. Commun. **54**, 409 (1989).

[10] S. Raman, C.H. Malarkey, W.T. Milner, C.W. Nestor, Jr., and P.H. Stelson, At. Data Nucl. Data Tables **36**, 1 (1987).

[11] A. Gavron, Phys. Rev. C **21**, 230 (1980).

[12] M. Dasgupta, A. Navin, Y.K. Agarwal, C.V.K. Baba, H.C. Jain, M.L. Jhingan, and A. Roy, Nucl. Phys. **A539**, 351 (1992).

[13] C.M. Lederer and V.S. Shirley, *Table of Isotopes* (Wiley-Interscience, New York, 1978).

[14] D. Ackermann, L. Corradi, D.R. Napoli, C.M. Petrache, P. Spolaore, A.M. Stefanini, F. Scarlassara, S. Beghini, G. Montagnoli, G.F. Segato, and C. Signorini, Nucl. Phys. **A575**, 374 (1994).

[15] J.F. Liang, L.L. Lee, Jr., J.C. Mahon, and R.J. Vojyech, Phys. Rev. C **50**, 1550 (1994).